RSC Advances

PAPER

View Article Online
View Journal | View Issue

Cite this: *RSC Adv.*, 2020, **10**, 41816

Ruddlesden–Popper phases of lithium-hydroxide-halide antiperovskites: two dimensional Li-ion conductors†

Anucha Koedtruad,[a] Midori Amano Patino,[a] Yu-Chun Chuang,[b] Wei-tin Chen,[c] Daisuke Kan[a] and Yuichi Shimakawa*[a]

Received 11th September 2020
Accepted 6th November 2020

DOI: 10.1039/d0ra07803d

rsc.li/rsc-advances

Lithium-oxide-halide and lithium-hydroxide-halide antiperovskites were explored for potential electrolytes in all-solid Li-ion batteries. A single-phase sample of the Ruddlesden–Popper (RP) series of compounds, $LiBr(Li_2OHBr)_2$ with double antiperovskite Li_2OHBr layers and rigid rock-salt type LiBr layers, was obtained. Li^+-ion vacancies are introduced in the double antiperovskite Li_2OHBr layers but not in the LiBr layers and induce two-dimensional Li-ion conduction with low activation energy by mediating Li-ion hopping. In contrast to the Br-containing RP phase, Cl-containing Li-oxide-halide and Li-hydroxide-halide RP phases cannot be crystallized due to the structural mismatch between the antiperovskite layers and rigid LiCl layers.

Introduction

All-solid Li-ion batteries are attracting interest due to their high energy densities and high voltage capabilities. The safe and thermally stable properties of solid electrolytes are also great advantages when compared with the properties of liquid electrolytes used in conventional Li-ion batteries.[1–4] Significant efforts have thus been made to develop solid-state Li-ion conducting electrolytes. The intensively studied electrolyte materials include oxides, sulfides, and polymers. However, there are still many obstacles for their practical implementations.[5–8]

Li-oxide halides and Li-hydroxide halides ($Li_{3-p}OH_pX$, $p = 0$–1, X = Cl and Br) with antiperovskite structures attract much attention recently as promising solid electrolytes. Although the Li-ion conductivity of the simple Li-oxide-halides antiperovskites was found to be low (10^{-9}–10^{-7} S cm^{-1} at room temperature), chemical manipulation by substitution with hydroxides increased the conductivity significantly.[9–12] For example, solid solution of $Li_3OCl_{1-x}Br_x$ and partial substitution of the constituent halide X ions with BH_4^- and F^- were also reported to increase the Li-ion conductivity.[13–16] Additional improvement in electrochemical window up to 9 V *versus* Li/Li$^+$ was found in F^- doped Li_2OHX (X = Cl and Br).[17]

We here focus on structural manipulation of the Li-oxide-halide and Li-hydroxide-halide antiperovskites by making layered-structure compounds. Ruddlesden–Popper (RP) series are known layered-structure phases based on the perovskite-structure materials, and many RP phases in oxides have been found.[18,19] We thus aim to synthesize the RP phases of the antiperovskites containing Li-oxide halides and Li-hydroxide halides. An RP phase of the antiperovskite, $LiX(Li_3OX)$, was recently computationally proposed to be a good Li-ion conductor.[20] The calculation suggested that an optimised $LiCl(Li_3OCl)$ structure included enlarged bottleneck space to facilitate the Li-ion hopping with a low barrier energy. And the molecular dynamics simulation indeed gave a high Li-ion diffusion coefficient. However, this phase has never been obtained experimentally. Although attempts were made to prepare $LiBr(Li_3OBr)_2$ and a minor phase of $LiBr(Li_3OBr)_2$ was found to be included in the Li_3OBr composition sample, it was difficult to isolate the pure RP phase.[21,22] In this study, we prepared a single-phase Li-hydroxide bromide with the RP structure and found that it shows high Li-ion conduction. Details of its crystal structure and Li-ion conductivity are discussed.

Experimental

The RP phase structures of the antiperovskites are considered as intergrowth layered structures consisting of LiX-rock-salt layers and the Li-oxide-halide-antiperovskite layers. The general formula is given as $LiX(Li_3OX)_n$, where n represents the number of antiperovskite layers stacked between LiX layers. Because Li-hydroxide halides ($Li_{3-p}OH_pX$) exhibit an enhanced Li-ion conductivity, RP phases with the Li-hydroxide-halide layers are also expected to be Li-ion conductors. We thus

[a]*Institute for Chemical Research, Kyoto University, Uji, Kyoto 611-0011, Japan. E-mail: shimak@scl.kyoto-u.ac.jp; Fax: +81-774-38-3118; Tel: +81-774-38-3110*

[b]*National Synchrotron Radiation Research Center, 101 Hsin-Ann Road, Hsinchu Science Park, Hsinchu 30076, Taiwan*

[c]*Center for Condensed Matter Sciences, National Taiwan University, No. 1, Sec. 4, Roosevelt Road, Taipei 10617, Taiwan*

† Electronic supplementary information (ESI) available. See DOI: 10.1039/d0ra07803d

synthesized samples with compositions of $LiX(Li_{3-p}OH_pX)_n$ with X = Br and Cl, $n = 1$, 2, and 3, and $p = 0$, 0.5, and 1 by solid-state reaction. The compositions cover the area shown in a ternary-phase diagram in Fig. 1.

The stoichiometric amounts of LiOH (98%, Alfa Aesar), Li_2O (>98%, Fujifilm Wako), and LiCl (>99%, Fujifilm Wako) or LiBr (>99.9%, Kojundo Chemical) were weighed and mixed well in a glovebox under an Ar atmosphere. Powder samples of the mixtures were placed in a glass tube and heated at 210–225 °C for 15 h. After cooling to room temperature, the samples were ground and reheated in the same condition for two times.

The phases of the synthesized samples were identified by a conventional X-ray diffraction (XRD) method with Cu-Kα radiation using the Bruker D8 ADVANCE diffractometer. Crystal structures were analyzed by using synchrotron X-ray diffraction (SXRD) data. The SXRD measurements were performed at the TPS09A beamline in Taiwan Photon Source with a wavelength of 0.82656 Å. The powder samples were packed into sealed glass capillary tubes and were rotated during the measurement to obtain better averaging of the observed intensities. Diffraction data were collected at temperatures from −153 to 207 °C. The obtained data were analyzed with the Rietveld method using the program RIETAN-VENUS.[23] The conductivity of the samples was measured by AC impedance spectroscopy using the Solatron1260 impedance analyzer and by the DC polarization method using the Keithley 2450 source-measure unit. The samples were pelletized into discs 10 mm in diameter and 3 mm thick, and for the conductivity measurements they were sandwiched by graphite electrodes. The AC impedance spectra at temperatures from room temperature to 80 °C were collected from 10 MHz to 1 kHz with an applied voltage of 0.1 V under N_2 gas flow. The DC polarization at room temperature was measured by applying a voltage of 0.1 V to complete polarization. The current as a function of time was collected.

Results and discussion

In the XRD patterns of prepared samples with X = Br (Fig. S1†), a characteristic diffraction peak originating from long-range layered order with $d \approx 5.39$ Å ($2\theta \approx 16.5°$) can be observed. This peak can be indexed as (0,0,4) and the d value corresponds to one fourth of the c axis length of the $n = 2$ RP phase (see the crystal structure in Fig. 2). Some of the diffraction peaks such as (1 0 5) at $2\theta \approx 30.5°$ and (1 1 0) at $2\theta \approx 31.5°$ in the patterns can also be indexed with the $n = 2$ RP phase. Although the diffraction peaks of the simple antiperovskite $Li_{3-p}OH_pBr$ were also included in the patterns except that of the $LiBr(Li_{2.5}OH_{0.5}Br)$ ($n = 1$ and $p = 0.5$) composition sample, characteristic diffraction peaks of the $n = 1$ and 3 RP layered structures were not observed. The results suggest that the $n = 2$ RP phase with X = Br can be crystalized but the other $n = 1$ and 3 RP phases are difficult to obtain under the present synthesis conditions. On the other hand, characteristic diffraction peaks of the RP layered structures were not seen in the patterns of the samples with X = Cl (Fig. S2†), indicating that none of the RP layered phases for the Cl-containing samples can be crystalized under the present synthesis conditions. The results are consistent with previous reports where only the $n = 2$ RP phase with Br was reported in multiphase samples and no Cl-containing RP phases have been reported.[21,22]

Importantly, from the diffraction pattern, the $LiBr(Li_{2.5}OH_{0.5}Br)$ composition appears to produce a single phase with no evident additional diffraction peaks from secondary phases. Then the crystal structure of the sample was analyzed with the SXRD data (Fig. 3). The observed diffraction pattern is essentially reproduced with the tetragonal ($I4/mmm$) structure model of the $n = 2$ RP phase (Fig. 2). Because H is insensitive to XRD, the initial model was thus set to be $LiBr(Li_3OBr)_2$, where double layers of the Li_3OBr antiperovskite are intercalated with rock-salt type LiBr layers. Given the O(4e) sites at the center of the Li octahedra are fully occupied, the refined occupancies for the

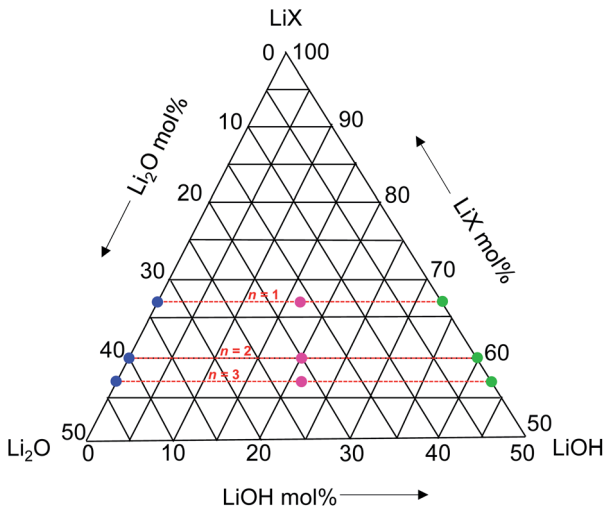

Fig. 1 Synthesized $LiX(Li_{3-p}OH_pX)_n$ compositions with X = Br and Cl, n = 1, 2, and 3, and p = 0, 0.5, and 1, presented in a ternary phase diagram.

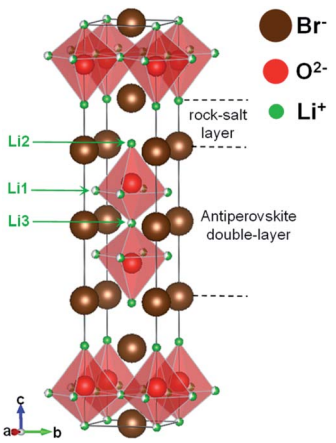

Fig. 2 Refined crystal structure of the $n = 2$ RP phase modeled as $LiBr(Li_3OBr)_2$. The actual experimental composition includes Li vacancies at the Li1 and Li3 sites, as well as hydroxide (OH) yielding the composition $LiBr(Li_2OHBr)_2$. The actual position of the H species cannot be determined by X-ray diffraction.

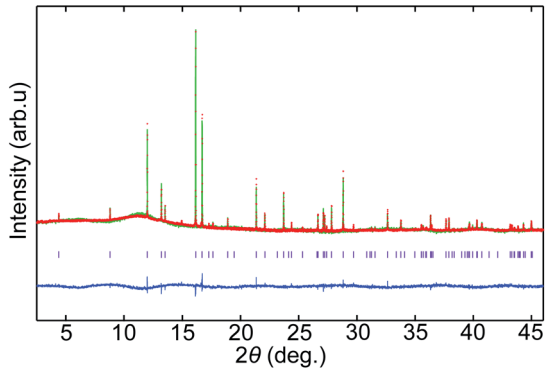

Fig. 3 SXRD pattern and the result of structural analysis for $LiBr(Li_2OHBr)_2$. The red markers and green solid line represent observed and calculated patterns, respectively. The blue line below is the difference between the observed and calculated intensities. The purple ticks are the allowed Bragg reflection positions for the structural model.

Br (2a and 4e) sites are also found to be fully occupied, and the occupancies for the sites were fixed to be 1.0. The refined occupancies for Li at the 8g, 4e, and 2a sites are respectively 0.59(4), 1.0, and 0.68(7). The final refinement results are listed in Table 1. The refinement results give a composition of $Li_5O_2Br_3$. Note that the Li occupancies for the Li1(8g) and Li3(2a) are significantly less than unity. Even though Li is also challenging to detect by XRD, these results suggest that some of the octahedra are Li deficient and instead H is introduced for making the Li-hydroxide-halide antiperovskite layers. Taking into account the charge neutrality condition, the most probable composition of the obtained single-phase sample would be $LiBr(Li_2OHBr)_2$, which is slightly different from, but close to, the target stoichiometry of the prepared sample. It is also interesting to note that the Li-ion vacancies at the octahedra are introduced not randomly but selectively and that rock-salt type LiBr layers are rigid.

As shown in the temperature-dependent SXRD (Fig. S3†), the $n = 2$ RP structure is stable at temperatures between −153 and 207 °C. No structural transition is observed in the measured temperature range.

Table 1 Refined structural parameters for the $LiBr(Li_2OHBr)_2$ $n = 2$ RP antiperovskite phase from room-temperature SXRD data. The H^+ ions have not been included in the model as they are not detectable by SXRD[a]

Atom	Site	x	y	z	g	B (Å^2)
Li1	8g	0	0.5	0.079(3)	0.59(4)	5.9(7)
Li2	4e	0	0	0.199(2)	1.0	5.9(7)
Li3	2a	0	0	0	0.68(7)	5.9(7)
O	4e	0	0	0.0994(7)	1.0	2.6(3)
Br1	2b	0	0	0.5	1.0	1.06(5)
Br2	4e	0	0	0.3123(1)	1.0	1.06(5)

[a] g is a site occupancy and B is an isotropic thermal parameter. The refined occupancies give a composition of $LiBr(Li_2OBr)_2$. Crystal structure; tetragonal, $I4/mmm$ space group, $a = 4.02363(3)$ Å, $c = 21.5736(2)$ Å, $V = 349.269(5)$ Å^3, $R_{wp} = 1.826\%$, and $R_p = 1.431\%$.

The rigid rock-salt type LiBr layers play an important role in stabilizing the RP phase and also explain why the Cl-containing RP phases were difficult to obtain. The large Br^- ions can easily be stabilized by the modified 9-fold coordination with the Li^+ ions in the rock-salt type layers. Additionally, the rock-salt type LiBr layer fits well to the Li-hydroxide (oxide) halide antiperovskite octahedra, as suggested by its tolerance factor $t = (r_{Cl/Br} + r_{Li})/\sqrt{2}(r_O + r_{Li}) = 0.90$, where r is an ionic radius for each constituent ion. In the Cl-containing compounds, on the other hand, Cl^- ions are too small to be located at the highly coordinated sites. The structural misfit between the rock-salt type layer and the antiperovskite layer ($t = 0.85$) makes the RP phases with Cl hard to synthesize.

Like the Li-hydroxide-halide antiperovskite, the present $n = 2$ RP phase $LiBr(Li_2OHBr)_2$ can be a Li-ion conductor. Although the conduction due to hopping of H^+ or OH^- can also be considered, the Li^+ conduction would be the most likely, as suggested in a previous report.[12] The conducting properties of the sample with the Nyquist plots of the impedance spectra are displayed in Fig. 4. The impedance, $Z = Z' - iZ''$, shows typical semi-circle behaviors at various temperatures, and the total conductivity (σ) is calculated from intersections at the real-part axes. The obtained conductivity at 30 °C is 1.27×10^{-7} S cm^{-1}, which is comparable to that of the simple antiperovskite Li_2OHBr (1.33×10^{-7} S cm^{-1}).[24] A DC polarization measurement at the same temperature (Fig. S4†) reveals that the electronic conductivity is of the order of 10^{-11} S cm^{-1}, which is about four orders of magnitude lower than the total conductivity. It is thus concluded that the electronic contribution to the conducting properties is very small and that the ionic conduction is dominant in the present $n = 2$ RP phase $LiBr(Li_2OHBr)_2$. The Arrhenius plot of temperature-dependent ionic conductivity shown in Fig. 5 gives the activation energy $E_a = 0.57$ eV by using the equation $\sigma = \sigma_0 \exp(-E_a/kT)$, where σ_0 is the conductivity pre-exponential factor, k is the Boltzmann constant, and T is the absolute temperature. This activation energy is similar to that of Li_2OHBr (0.55 eV).[24]

We note again that the Li vacancies are introduced in the Li1 and Li3 sites and that the rock-salt type LiBr layer is rigid. This implies that Li-ion hopping conduction through the vacant sites

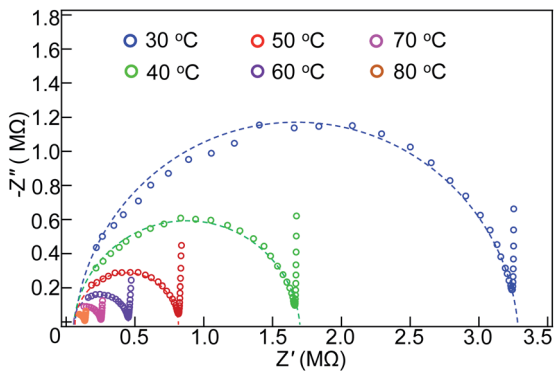

Fig. 4 Nyquist plots from impedance spectroscopy measurements of the $n = 2$ RP phase $LiBr(Li_2OHBr)_2$ antiperovskite at various temperatures.

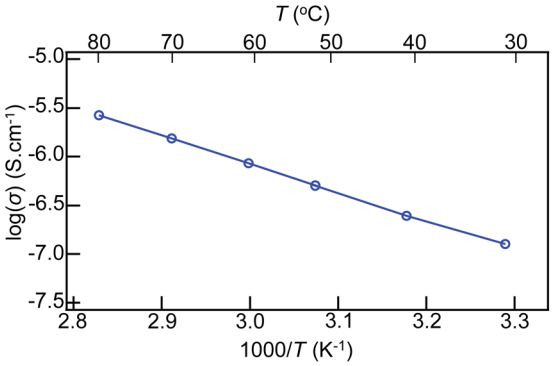

Fig. 5 Temperature dependence of ionic conductivity for $LiBr(Li_2OHBr)_2$.

are confined within the two-dimensional double antiperovskite layers. Interlayer hopping between the rigid LiBr layers should need high activation energies and thus are less likely to occur, leading to almost no Li-ion conduction along the stacking layer. The observed low activation energy for the present $n = 2$ RP antiperovskite phase, which is comparable to that of the simple antiperovskite Li_2OHBr, is also consistent with the conduction only of the antiperovskite layers. Because the present Li-ion conductivity was measured in a polycrystalline sample, the actual (intrinsically two-dimensional) ionic conductivity within the antiperovskite layers in the RP phase is expected to be much larger than that measured here.

Conclusions

We synthesized the Li-oxide-halide and Li-hydroxide-halide antiperovskites $LiX(Li_3OX)_n$ and $LiX(Li_{3-p}OH_pX)_n$ (X = Br and Cl) by solid-state reactions. We identified the phases and analyzed their crystal structures by SXRD. We found that the $n = 2$ layered RP phase of Li-hydroxide-bromide antiperovskite $LiBr(Li_2OHBr)_2$ crystallizes in the *I*4/*mmm* tetragonal structure, which consists of double layers of the Li_2OHBr antiperovskite between rock-salt-type LiBr layers. Li^+-ion vacancies were introduced selectively in antiperovskite layers, and the rock-salt type LiBr layers were rigid. The RP structure is stabilized by the large Br^- ions coordinated with 9 Li^+ ions and by the lattice match between the rock-salt LiBr type layer and the Li-hydroxide-bromide antiperovskite layer. The RP phases with Br, $n = 1$, 3, and Cl, $n = 1$, 2, 3, were not stable.

The Li^+ vacancies revealed in the $n = 2$ RP phase $LiBr(Li_2OHBr)_2$ promote the Li-ion conduction and the compound shows ionic conductivity of 1.27×10^{-7} S cm^{-1} at 30 °C with an activation energy of 0.57 eV. Because the rigid rock-salt type LiBr layers contribute less in the Li-ion hopping, Li^+ ions primarily migrate within the double antiperovskite layers, leading to the two-dimensional ion conduction. The intrinsic two-dimensional Li^+-ion conductivity may be much higher than that observed. The present results demonstrate that the novel RP phases of antiperovskite halides have great potential for developing highly conductive Li-ion conductors with thermally stable properties.

Conflicts of interest

There are no conflicts to declare.

Acknowledgements

We thank Dr Masato Goto, Zhenhong Tan and Yoshihisa Kosugi for help in experiments. The synchrotron radiation experiments were performed at the National Synchrotron Radiation Research Center (proposal No. 198). This work was partly supported by Grants-in-Aid for Scientific Research (No. 16H02266, 17K19177, 19H05816, 19K23650, and 20H00397) and by grants for the Integrated Research Consortium on Chemical Sciences and the International Collaborative Research Program of Institute for Chemical Research in Kyoto University from the Ministry of Education, Culture, Sports, Science and Technology (MEXT) of Japan. This work was also supported by the Japan Society for the Promotion of Science Core-to-Core Program (A) Advanced Research Networks.

References

1 Q. Li, J. Chen, L. Fan, X. Kong and Y. Lu, *Green Energy Environ*, 2016, **1**, 18–42.
2 A. Manthiram, X. Yu and S. Wang, *Nat. Rev. Mater.*, 2017, **2**(4), 16103.
3 T. Famprikis, P. Canepa, J. A. Dawson, M. S. Islam and C. Masquelier, *Nat. Mater.*, 2019, **18**, 1278–1291.
4 Q. Yang and C. Li, *Energy Storage Materials*, 2018, **14**, 100–117.
5 P.-J. Lian, B.-S. Zhao, L.-Q. Zhang, N. Xu, M.-T. Wu and X.-P. Gao, *J. Mater. Chem. A*, 2019, **7**, 20540–20557.
6 Z. Gao, H. Sun, L. Fu, F. Ye, Y. Zhang, W. Luo and Y. Huang, *Adv. Mater.*, 2018, **30**, 1705702.
7 S. Ohno, A. Banik, G. F. Dewald, M. A. Kraft, T. Krauskopf, N. Minafra, P. Till, M. Weiss and W. G. Zeier, *Prog. Energy*, 2020, **2**, 022001.
8 X. Li, J. Liang, X. Yang, K. R. Adair, C. Wang, F. Zhao and X. Sun, *Energy Environ. Sci.*, 2020, **13**, 1429–1461.
9 X. Lü, G. Wu, J. W. Howard, A. Chen, Y. Zhao, L. L. Daemen and Q. Jia, *Chem. Commun.*, 2014, **50**, 11520–11522.
10 I. Hanghofer, G. J. Redhammer, S. Rohde, I. Hanzu, A. Senyshyn, H. M. R. Wilkening and D. Rettenwander, *Chem. Mater*, 2018, **30**, 8134–8144.
11 A.-Y. Song, Y. Xiao, K. Turcheniuk, P. Upadhya, A. Ramanujapuram, J. Benson, A. Magasinki, M. Olguin, L. Meda, O. Borodin and G. Yushin, *Adv. Energy Mater.*, 2018, **8**, 1700971.
12 J. A. Dawson, T. S. Attari, H. Chen, S. P. Emge, K. E. Johnston and M. S. Islam, *Energy Environ. Sci.*, 2018, **11**, 2993–3002.
13 Y. Zhao and L. L. Daemen, *J. Am. Chem. Soc.*, 2012, **134**, 15042–15047.
14 Z. Deng, B. Radhakrishnan and S. P. Ong, *Chem. Mater.*, 2015, **27**, 3749–3755.
15 H. Fang, S. Wang, J. Liu, Q. Sun and P. Jena, *J. Mater. Chem. A*, 2017, **5**, 13373–13381.

16 H. Fang and P. Jena, *Proc. Natl. Acad. Sci. U.S.A.*, 2017, **114**, 11046–11051.
17 Y. Li, W. Zhou, S. Xin, S. Li, J. Zhu, X. Lu, Z. Cui, Q. Jia, J. Zhou, Y. Zhao and J. B. Goodenough, *Angew. Chem., Int. Ed.*, 2016, **55**, 9965–9968.
18 B. V. Beznosikov and K. S. Aleksandrov, *Crystallography Report*, 2000, **45**, 792–798.
19 G. Nirala, D. Yadav and S. Upadhyay, *J. Adv. Ceram.*, 2020, **9**, 129–148.
20 Z. Lu, J. Liu and F. Ciucci, *Energy Storage Materials*, 2020, **28**, 146–152.
21 J. Zhu, S. Li, Y. Zhang, J. W. Howard, W. Lu, Y. Li, Y. Wang, R. S. Kumar, L. Wang and Y. Zhao, *Appl. Phys. Lett.*, 2016, **109**, 101904.
22 K. Friese, A. Honnerscheid and M. Jansen, *Z. Kristallogr.*, 2003, **218**, 536–541.
23 F. Izumi and K. Momma, *Solid State Phenom*, 2007, **130**, 15–20.
24 A. Koedtruad, M. A. Patino, N. Ichikawa, D. Kan and Y. Shimakawa, *J. Solid State Chem.*, 2020, **286**, 121263.